Chapter 5
AVO Analysis

5.1 AVO analysis of the surface seismic data

The AVO characters of gas sands, wet sands and coal beds of the surface seismic data were analyzed on two CDP gathers at Well C (Figure 5.1 and 5.2). Figure 5.1 is the reprocessed CDP gather 286 after phase rotation on line A showing picked seismic events and the three propagation angle bands: near offset, middle offset, and far offset. Figure 5.2 shows the CDP gather 349 after phase rotation on line B.

All gas sands (Gas sand A, B, C, and D) show strong amplitude level on the both lines. They show positive AVO trends up to middle offset on line A but up to the far offset on line B except for gas sand A, which show relatively flat AVO trends. The gas sand B and D on line A show discontinuous reflector amplitude in the near offset, however in the middle and far offset they show the continuity. The wet sand B and D on line B show strong amplitude level throughout all offsets with positive AVO trends while wet sands A and C show weak amplitude level with relatively flat AVO trends. All wet sands on line A show weak to moderate amplitude level with rather flat AVO trends. All coal beds (Coal bed A, B and C) on line B show weak amplitude level with rather flat to negative AVO trends. On line A coal beds A and B show relatively weak amplitude level with negative AVO trends while coal bed C shows strong amplitude with positive AVO trend.

Figure 5.3 shows the amplitude cross-plot between near-offset stack (0-15°) and far-offset stack (30°-45°) at CDP gather 349 on line B. It can be seen that each lithologic unit gives a separate cluster group enabling unique identification or prediction of different fluid types. Gas sands show relatively the highest amplitudes at near and far offsets. Wet sands show another group with values generally lower than those of gas sands. Coal beds show the lowest far-offset amplitudes. Table 5.1 shows the real amplitude values picked and plotted in Figure 5.3. The gas sands A and B give increasing amplitudes at far offset, while the gas sands C and D show decreased amplitudes. All the four wet sands give increasing amplitudes with offsets,

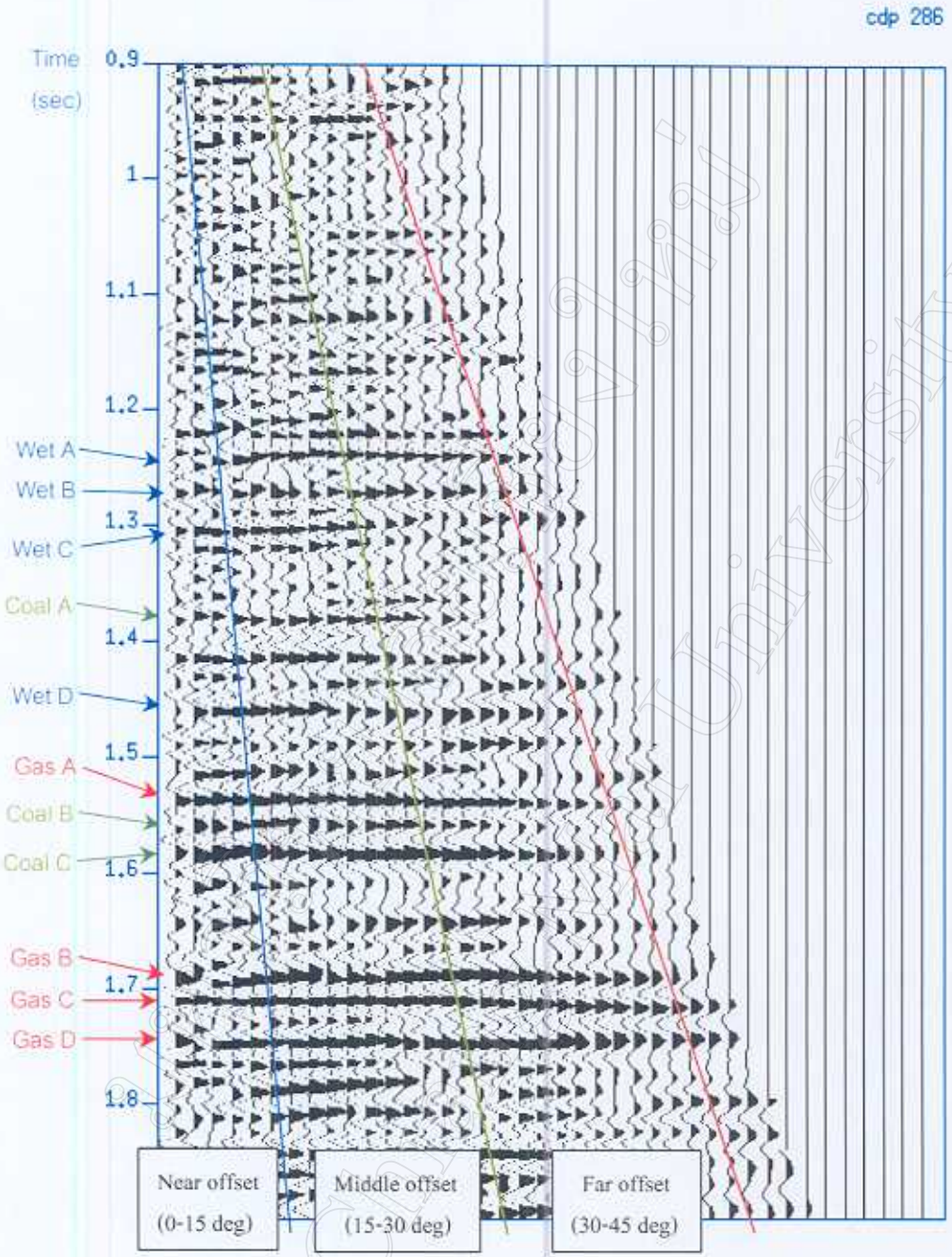

Figure 5.1 CDP gather 286 on line A after phase ratation showing the seismic marker events and the three propagation angle bands.

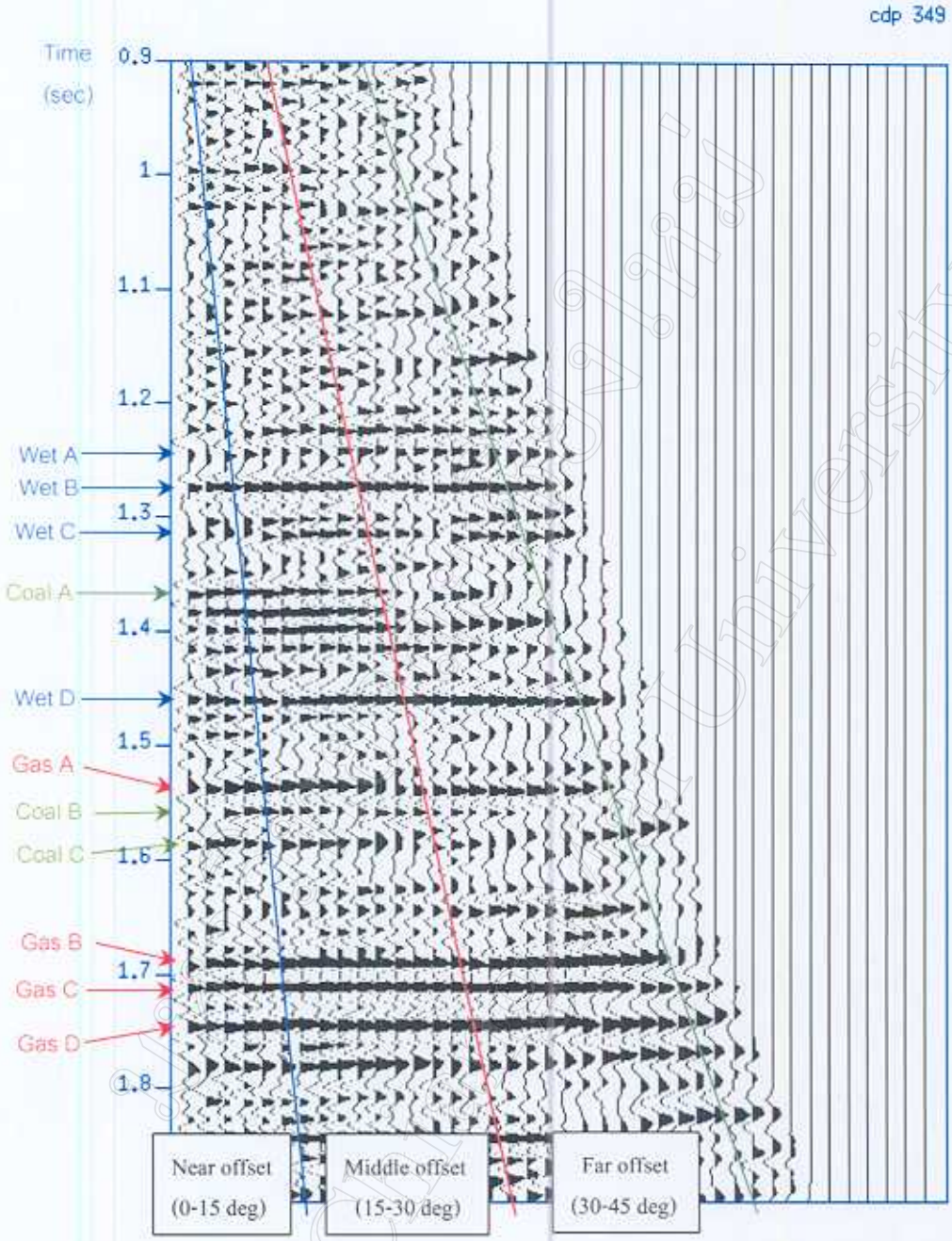

Figure 5.2 CDP gather 349 on line B after phase rotation showing the seismic marker events and the three propagation angle bands.

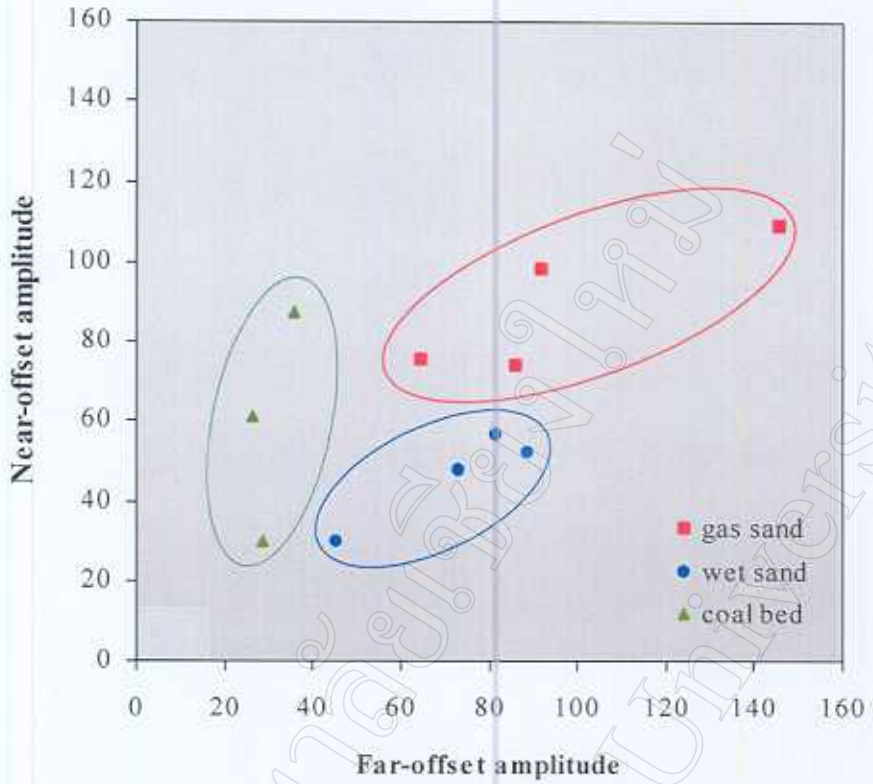

Figure 5.3 Amplitude cross-plot between near-offset and far-offset stacks at CDP gather 349 on line B..

Table 5.1 Amplitude values picked from near-angle and far angle stacks at CDP gather 349 on line B.

Lithologic unit	Near-offset amplitude	Far-offset amplitude
Gas sand A	73.950	85.848
Gas sand B	109.200	145.800
Gas sand C	75.714	64.602
Gas sand D	98.492	91.707
Wet sand A	47.474	72.933
Wet sand B	56.692	81.530
Wet sand C	29.599	45.336
Wet sand D	52.297	88.672
Coal bed A	87.209	35.905
Coal bed B	60.995	26.478
Coal bed C	29.688	28.634

while all the coal beds give decreasing amplitudes with offsets. The stacking process might distort wavelet shapes that could be a cause of minor AVO variations.

5.2 Elastic impedance for AVO analysis

The idea of elastic impedance associated with AVO analysis and inversion is well established by now. In general, if different fluid types and/or lithology would be separately clustered on a cross-plot of far-angle and near-angle elastic impedances (zero-offset EI is identical to AI), then an AVO inversion could work for lithology and/or fluid-type predictions.

Figure 5.4 shows the relationship between far-angle elastic impedance EI(25) and near-angle elastic impedance EI(10). Figure 5.5 shows the relationship between EI (25) and acoustic impedance AI. It can be seen that each lithologic unit shows a separate group of cross-relationship. The gas sands have high acoustic impedance and high near-angle elastic impedance, but the lowest far-angle elastic impedance. The wet sands have high acoustic and near-angle elastic impedances but low far-offset elastic impedance. The far-offset elastic impedance values of wet sands are higher than those of gas sands but lower in acoustic and near-offset elastic impedances. The coal beds have the group of highest far-offset elastic impedance but lowest near-offset elastic and acoustic impedances. These different groups of cross-relationship indicate that the gas sands, wet sands, and coal beds in this study area have different AVO characteristics.

5.3 Acoustic impedance and reflection coefficient relationship

The acoustic impedance and normal-incident reflection coefficient relationship of the selected lithologic units in Table 2.3 is shown in Figure 5.6. This is the top-interface normal-incident reflection coefficient and acoustic impedance relationship. The relationship between the bottom-interface reflection coefficient and acoustic impedance is shown in Figure 5.7. Table 5.2 shows the velocity and density parameters for the bottom lithologic units. The relationship between those reflection coefficients and the acoustic impedance show a separate group for each lithologic unit. The gas sands show a group of lowest absolute-reflection coefficient but highest acoustic impedance, while the coal beds show a group of highest absolute-reflection

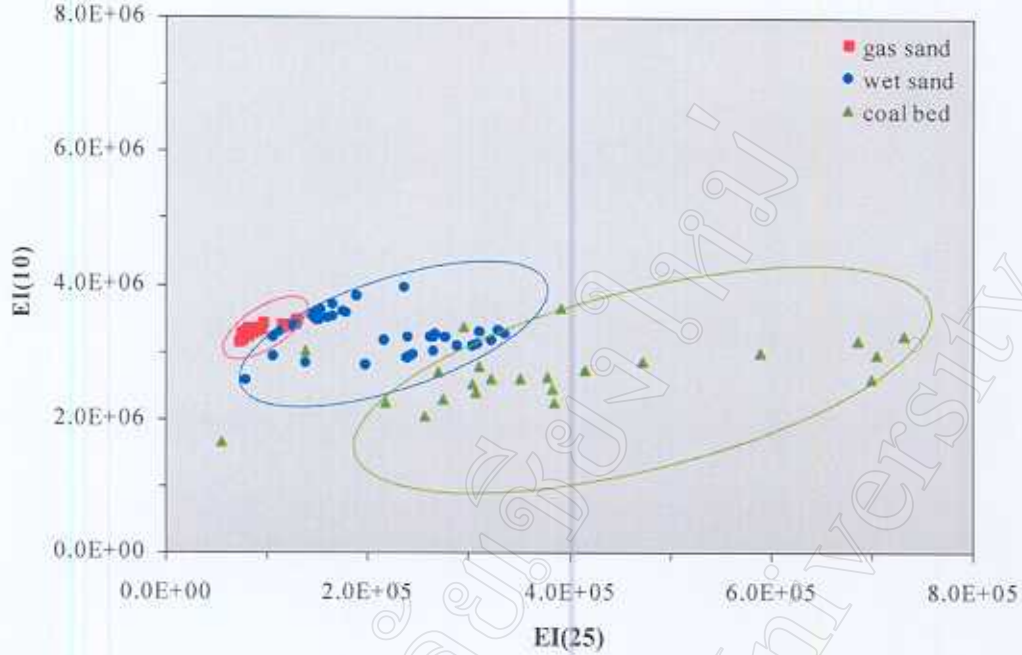

Figure 5.4 Cross-plot of elastic impedances at near-angle, EI(10) and far-angle, EI(25)..

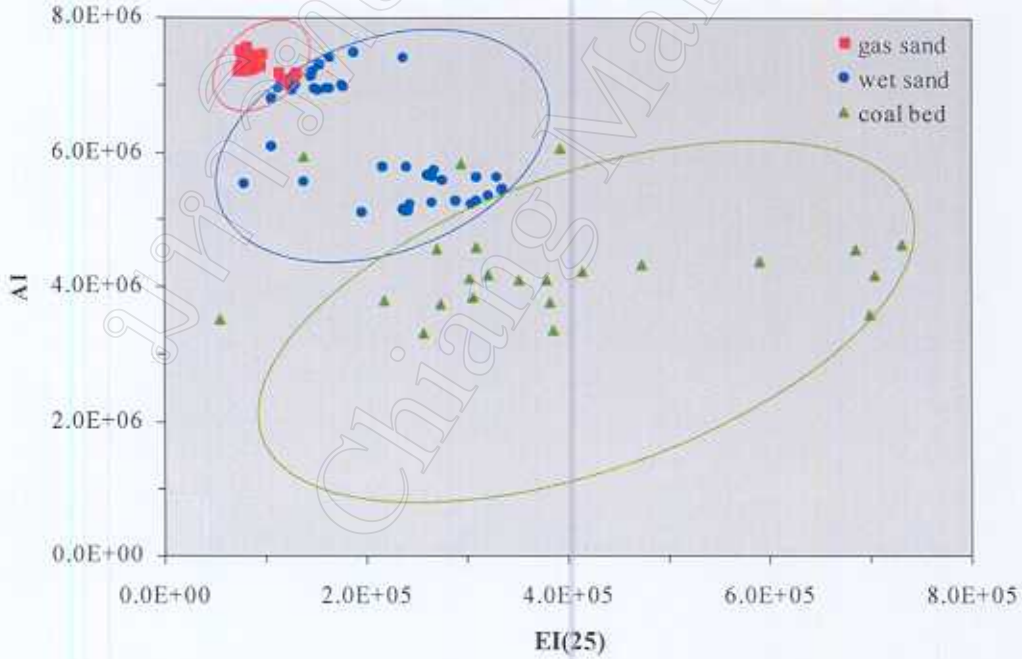

Figure 5.5 Cross-plot of acoustic impedance, AI and far-angle elastic impedance, EI(25).

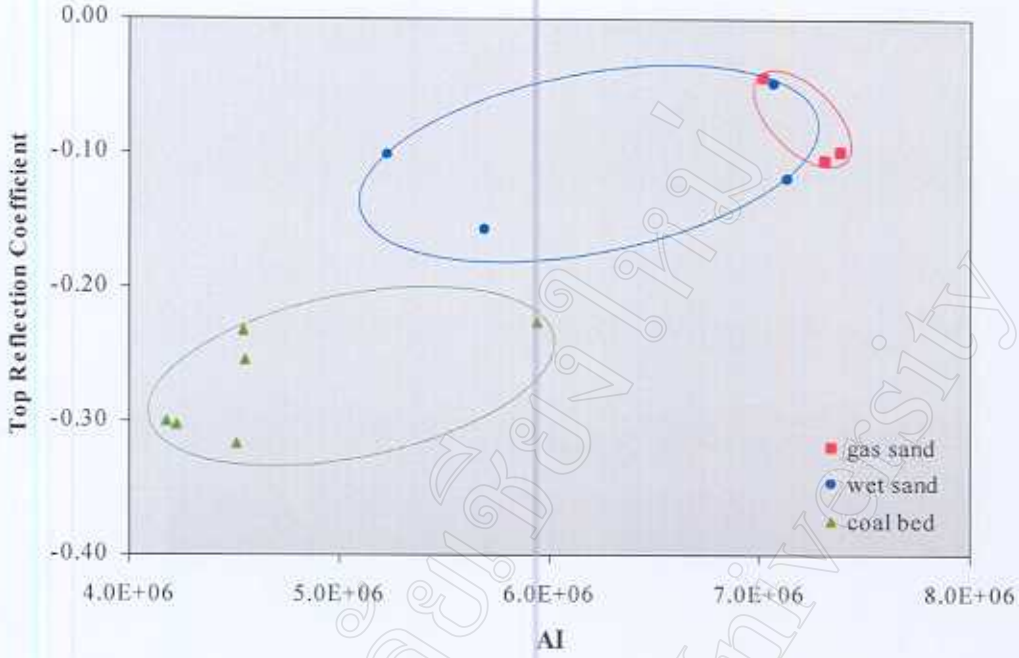

Figure 5.6 Acoustic impedance and top reflection coefficient relationship.

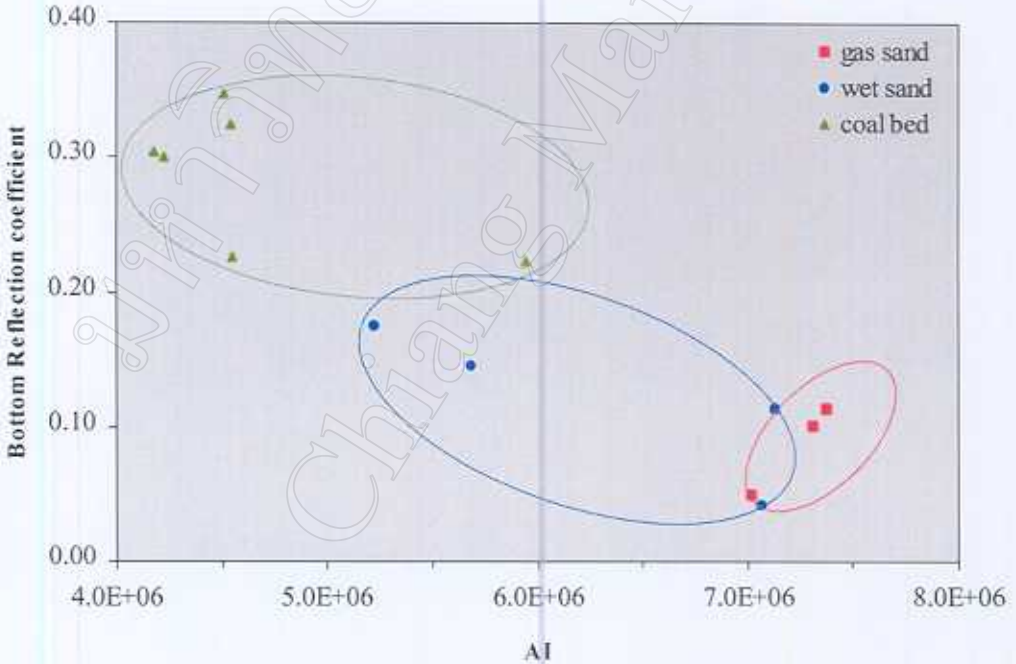

Figure 5.7 Acoustic impedance and bottom reflection coefficient relationship.

Table 5.2 Velocity and density parameters for bottom lithologic units.

Unit layer	Vp(m/s)	Density(g/cc)
gas 1	3214.3	2.184
(shale)	3320.9	2.338
gas 2	3308.7	2.230
(shale)	3557.7	2.609
gas 3	3305.5	2.212
(shale)	3508.6	2.555
wet 1	2547.4	2.052
(shale)	3051.3	2.438
wet 2	2748.8	2.070
(shale)	3171.1	2.409
wet 3	3201.1	2.207
(shale)	3111.8	2.473
wet 4	3218.4	2.215
(shale)	3712.3	2.411
coal 1	2544.4	1.788
(shale)	3009.3	2.393
coal 2	2577.4	1.621
(shale)	3207.0	2.442
coal 3	2542.6	1.664
(shale)	3300.9	2.379
coal 4	2689.1	1.691
(shale)	3538.3	2.521
coal 5	2635.2	1.711
(shale)	3675.0	2.538
coal6	2982.5	1.993
(shale)	3636.6	2.575

coefficient but lowest acoustic impedance. The wet sands show a group of moderate to high absolute-reflection coefficient and acoustic impedance. These relationships are related to tuning and composite AVO responses for thin sands.

5.4 P-wave and S-wave velocity relationship

Using the V_p and V_s from Well C, the V_p and V_s linear-regression relationships for gas sands, wet sands, coal beds and shale are computed. The linear-regression relationship equation of each lithology is shown in Table 5.3. The V_p and V_s relationship of gas sands are shown in Figure 5.8. Figures 5.9, 5.10, and 5.11 show that of wet sands, coal beds and shale, respectively.

It can be seen that the gas sands for this study area have the highest S-wave velocities. The wet sands and shale have medium to high S-wave velocities but lower than that of the gas sands. The coal beds have the lowest S-wave velocities. The differences in S-wave velocity cause the differences in AVO responses for each unit layer.

These linear regression relationships between V_p and V_s of different rocks could be utilized for the AVO analysis at the locations where no DSI log was acquired (it is so common that the main log suite does not include DSI but regular P-wave sonic and density).

Table 5.3 The V_p and V_s linear-regression relationship equations for gas sands, wet sands, coal beds, and shale.

Lithology	V_p-V_s relationship
Gas sands	$V_s = 0.8355V_p - 0.7438$
Wet sands	$V_s = 0.7601V_p - 0.5515$
Coal beds	$V_s = 0.4607V_p + 0.1328$
Shale	$V_s = 0.7519V_p - 0.8019$

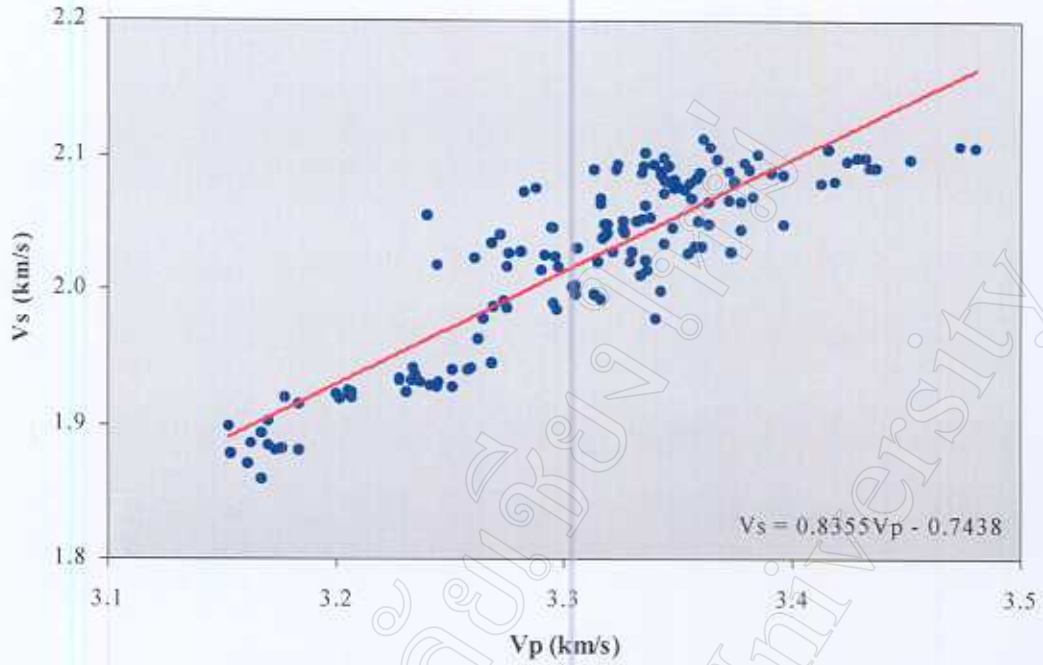

Figure 5.8 Vp-Vs relationship for gas sands at Well C.

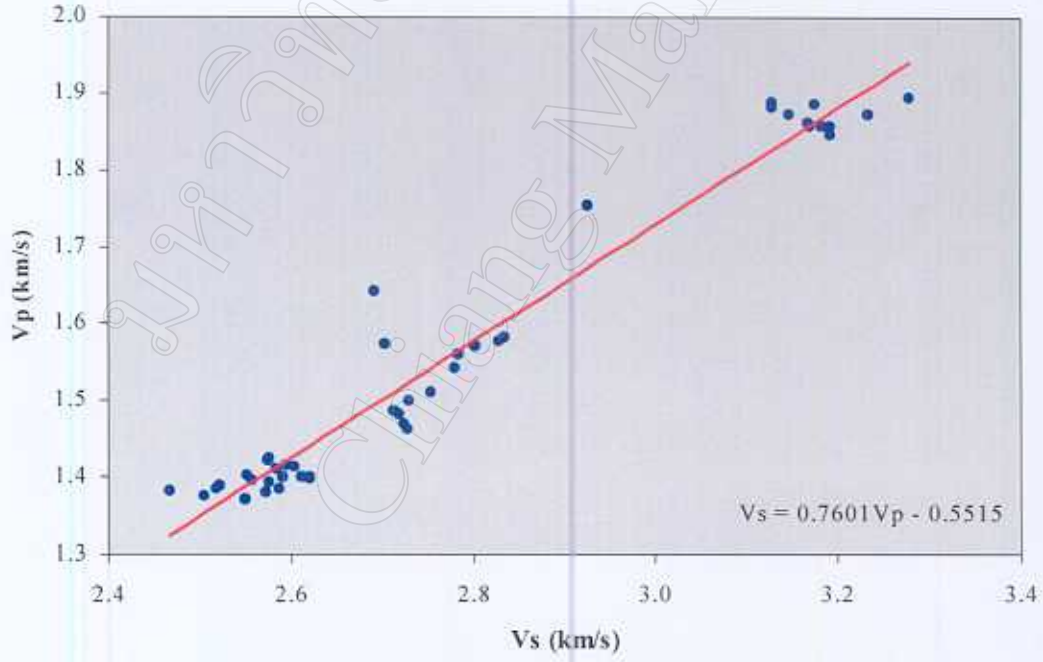

Figure 5.9 Vp-Vs relationship for wet sands at Well C.

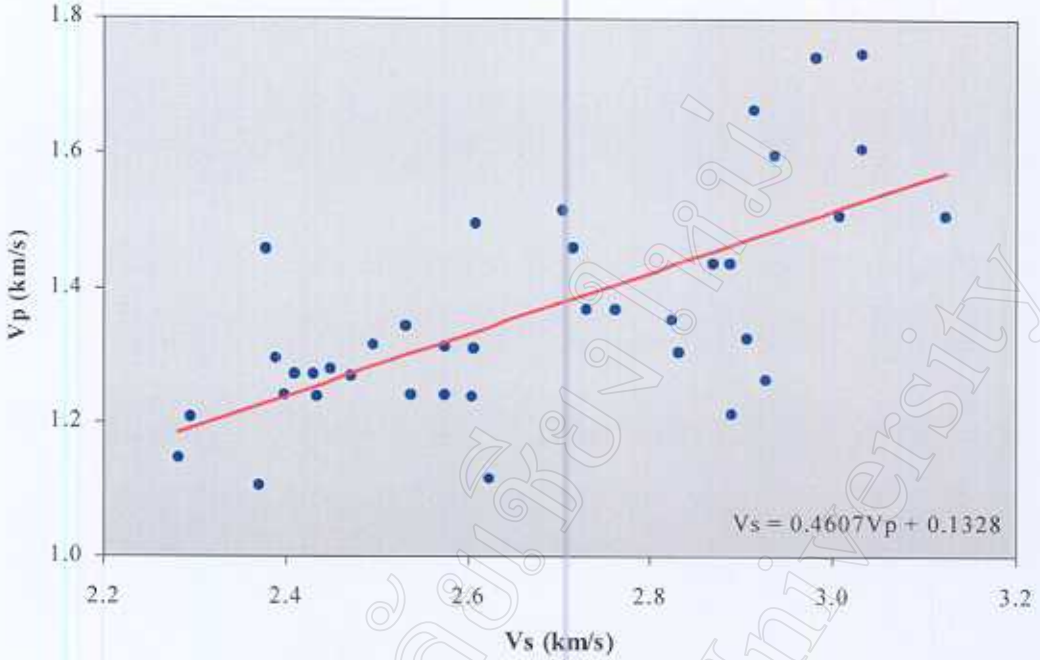

Figure 5.10 Vp-Vs relationship for coal beds at Well C.

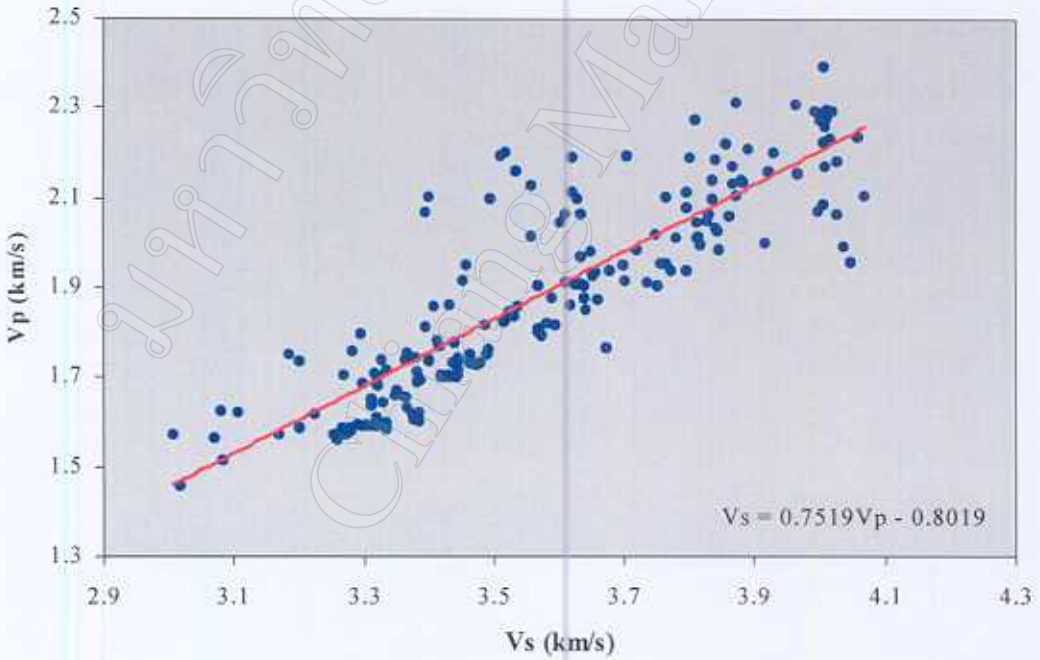

Figure 5.11 Vp-Vs relationship for shale at Well C.